Journal of Solid State Chemistry 183 (2010) 2082–2086

Contents lists available at ScienceDirect

Journal of Solid State Chemistry

journal homepage: www.elsevier.com/locate/jssc

Polymorphism of new rubidium magnesium monophosphate

Rajia Ait Benhamou [a,b], Gilles Wallez [a,*], Pascal Loiseau [a], Bruno Viana [a], Mohamed Elaatmani [b], Mohamed Daoud [b], Abdelwahed Zegzouti [b]

[a] Laboratoire de Chimie de la Matière Condensée de Paris, CNRS-UMR7574, ENSCP-ParisTech, UPMC University Paris 06, 11 rue Pierre et Marie Curie, 75231 Paris Cedex 05, France
[b] Laboratoire de la Matière Condensée et de l'Environnement, Université Cadi Ayyad, Faculté des Sciences-Semlalia, Marrakech, Morocco

ARTICLE INFO

Article history:
Received 10 May 2010
Received in revised form
24 June 2010
Accepted 10 July 2010
Available online 17 July 2010

Keywords:
Phosphates
Crystal structure
Rietveld analysis
Phase transitions

ABSTRACT

Novel phase $RbMgPO_4$, synthesized by solid state reaction, sustains phase transitions at 169 and 184 °C. The medium (β)- and high- (γ) temperature forms (orthorhombic, respectively $Pna2_1$ and $Pnma$, $Z=4$) are typical stuffed tridymites but the ambient form (α) exhibits an unusual three-fold $Pna2_1$ superstructure that results from the change of coordination of one third of the Mg atoms. Cell parameters are as follows: for α: $a=26.535(1)$ Å, $b=9.2926(3)$ Å, $c=5.3368(2)$ Å; for β: $a=8.7938(3)$ Å, $b=9.3698(3)$ Å, $c=5.3956(1)$ Å; for γ: $a=8.7907(3)$ Å, $b=5.4059(1)$ Å, $c=9.3949(3)$ Å.

1. Introduction

The $ABPO_4$ phosphates with big A^I cations and B^{II} in tetrahedral environment belong to a wide structural family in which the BPO_4^- tetrahedra framework shows four-, six- and eight-membered rings, not unlike some silica or silicate forms. The tunnels perpendicular to the six-membered rings form irregular open cavities that host the monovalent cation. Depending on the ionic radius of A^I, various morphologies are observed, for which the most convenient descriptive parameter is the up/down sequence of the tetrahedra perpendicular to the six-membered rings, to be compared to the UDUDUD pattern of tridymite SiO_2, and therefore these compounds are commonly known as "stuffed tridymites". Structural modifications are necessary to accommodate the A^I cation: medium-size K^I tends to preserve partly the UD alternation, along with the ternary/senary symmetry, like in hexagonal $KZnPO_4$ (UUUDDD/UDUDUD: 3/1) [1], but in most cases, K^I, along with bigger Tl^I, Rb^I and Cs^I, strongly distort the oxygen cages, thus forming fully UUUDDD rings with lower symmetries [2–7].

The works of Blum et al. [3,4] on $CsZnPO_4$ and $CsCoPO_4$ have revealed the typical thermal evolution of the UUUDDD phosphates: double-cell ($Z=8$) $P2_1/c$, single-cell ($Z=4$) $Pna2_1$ and $Pnma$ successively on heating, i.e., the same polymorphism as that of isotopic NH_4LiSO_4 [8–10]. The transition points are strongly dependent on the cations sizes, and therefore the compounds of this family can adopt either of these space groups at room temperature, i.e., $Pna2_1$ for $KBePO_4$ [2] and $TlBePO_4$ [11], $Pnma$ for $CsMgPO_4$ [5]. A strong peak of the dielectric constant around the Curie point accounts for the ferroelectric character of the $Pna2_1$–$Pnma$ (with b–c axes permutation) transition in $CsZnPO_4$ [3,4] and $TlBePO_4$ [11]; in the latter, the polarization effect of the Tl^I $6s^2$ lone pair and its effect on ferroelectricity have been evidenced [7].

Till date, few studies have been dedicated to the M^IMgPO_4 compounds, but it already appears that the monovalent cation plays a strong steric effect by shifting the temperatures of the phase transitions inversely to its size: monoclinic $KMgPO_4$ sustains the two modifications at 362 and 422 °C [12], whereas $CsMgPO_4$ is orthorhombic $Pnma$ at room temperature [5], with two potential (but not yet observed) transitions at lower temperatures. Owing to the intermediate radius of Rb^I compared to those of K^I and Cs^I, $RbMgPO_4$ could conceivably undergo these transitions at positive but moderate temperatures, which could be particularly interesting concerning the ferroelectric phenomenon. The study of this novel compound has been undertaken in this scope.

2. Experimental

$RbMgPO_4$ was synthesized by the solid state reaction from previously dried powders of Sigma-Aldrich reagents in stoichiometric amounts: Rb_2CO_3 (99%), $4MgCO_3 \cdot Mg(OH)_2 \cdot 5H_2O$ (99%) and $(NH_4)_2HPO_4$ (98.5%). The ground mixture was heated from ambient temperature to 400 °C at a 1 °C/min, ground again and finally annealed 12 h at 900 °C. Differential thermal analysis

* Corresponding author. Fax: +33 1 46 34 74 89.
E-mail address: gilles.wallez@upmc.fr (G. Wallez).

0022-4596/$ - see front matter © 2010 Elsevier Inc. All rights reserved.
doi:10.1016/j.jssc.2010.07.016

(DTA) was performed on a Setaram 92 analyzer at a 300 °C h^{-1} heating rate.

A cylindrical pellet was made by uniaxial pressing of $RbMgPO_4$ powder mixed with 2 wt% Bi_2O_3 as a flux and ethanol, then heated at 1000 °C for 2 h. Compaction of 78% was obtained. Silver lacquer was deposited on the faces of the so-obtained ceramic. High temperature dielectric measurements were performed with an automated Hewlett–Packard (HP4284A, 20 Hz–1 MHz) spectrometer at a 180 °C h^{-1} heating rate.

The room temperature diffraction pattern was recorded on a Panalytical X'Pert Pro diffractometer with an incident-beam Ge monochromator, at $U=45$ kV and $I=40$ mA (other acquisition parameters are summarized in Table 1). The apparatus was equipped with an Anton Paar HTK 1200 N furnace for high temperature diffraction. The Rietveld structural analyses were made using the Fullprof suite [13].

3. Results and discussion

The DTA, high-temperature dielectric measurements (Fig. 1) and thermal expansion curves inferred from XRD measurements (Fig. 2) account for two phase transitions starting at 169 and 184 °C (DTA measurement). The three varieties will be termed γ (high T), β (medium T) and α (low T).

3.1. γ-$RbMgPO_4$

The diffraction pattern collected at 220 °C is typical of an orthorhombic $Pna2_1$ or $Pnma$ stuffed tridymite. The Rietveld refinement was initiated with the lowest symmetry ($Pna2_1$) using the structural data of $TlBePO_4$ [7]. Soft constraints were applied to the P–O distances. The so-obtained atomic positions evidenced a supplementary m-mirror that led to upgrade the symmetry to $Pnma$, as expected for a HT prototype form. The new refinement did not increase the reliability factors significantly. Analysis conditions are reported in Table 1, atomic positions in Table 2 and cation–anion distances in Table 3. For crystal structure, see Fig. 3 (top). The strong thermal parameters of oxygen atoms O1 and O2 and the anomalous short Mg–O1 and –O2 distances are typical effects of the rocking of oxygens perpendicular to the Mg–P direction. This transverse motion is made possible by the soft Rb–O1 and –O2 bonds, whereas O3, closer to the neighbor Rb's (3.02 and 3.12 Å), cannot rock significantly. This phenomenon,

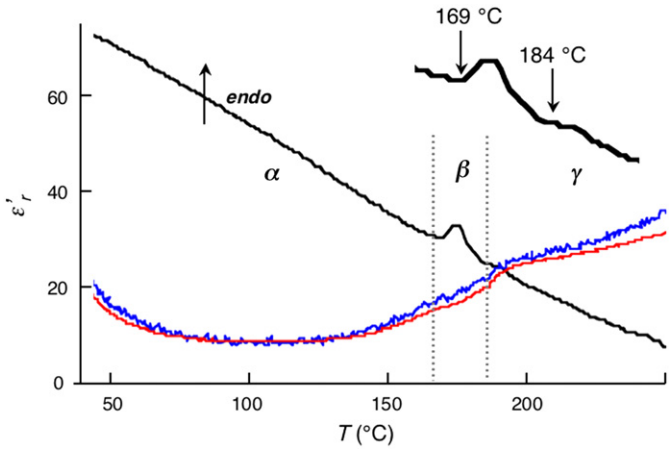

Fig. 1. DTA plot (black, arbitrary scale) and thermal evolution of the dielectric permittivity (blue: 500 kHz, red: 1 MHz) of $RbMgPO_4$. (For interpretation of the references to color in this figure legend, the reader is referred to the web version of this article.)

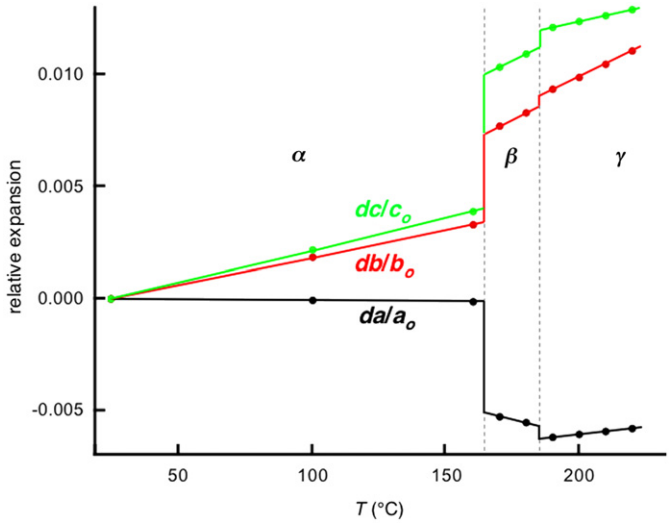

Fig. 2. Relative thermal expansion curves of the $RbMgPO_4$ cell edges measured by high temperature diffraction and Rietveld analysis. a, b and c refer to the cell edges of the β-form (for α, a has to be tripled, for γ, b and c have to be permuted). Error bars are smaller than the dot size.

Table 1
Data collection, refinement conditions and crystallographic data for the three forms of $RbMgPO_4$.

Phase	γ-$RbMgPO_4$	β-$RbMgPO_4$	α-$RbMgPO_4$
Temperature (°C)	220	180	25
2θ range/step (°)	10–130/0.013	10–130/0.013	10–140/0.013
Total counting time (h)	5	5	12
Number of Bragg reflections	435	436	1421
Number of I-dependent parameters	20	28	69
$R_P = \sum \lvert y_o^i - y_c^i \rvert / \sum y_o^i$	0.08	0.077	0.044
R_{WP} (id, weighted)	0.10	0.10	0.063
$R_{Bragg} = \sum \lvert I_o^i - I_c^i \rvert / \sum I_o^i$	0.066	0.057	0.044
$R_{exp} = ((n-p)/\sum w_i y_o{}^i)^{1/2}$	0.081	0.08	0.032
$R_F = \sum \lvert (I_o^i)^{1/2} - (I_c^i)^{1/2} \rvert / \sum (I_o^i)^{1/2}$	0.11	0.10	0.040
$\chi^2 = (R_{WP}/R_{exp})^2$	1.87	1.75	3.75
Space group	$Pnma$	$Pna2_1$	$Pna2_1$
a (Å)	8.7907(3)	8.7938(3)	26.535(1)
b (Å)	5.4059(1)	9.3698(3)	9.2926(3)
c (Å)	9.3949(3)	5.3956(1)	5.3368(2)
V (Å^3)/Z	446.46(4)	444.58(4)	1316.0(1)/12
Density (calc.)	3.05	3.06	3.11

Table 2
Positional and isotropic thermal parameters of the three forms of $RbMgPO_4$.

Atom	x	y	z	B_{iso} (Å^2)
γ-RbMgPO$_4$ (220 °C)				
Rb	−0.0018(4)	1/4	0.3067(1)	3.76(4)
Mg	0.3272(6)	1/4	0.5785(7)	5.4(2)
P	0.3000(3)	3/4	0.4110(4)	2.08(9)
O1	0.205(2)	3/4	0.273(1)	12.9(5)
O2	0.4728(5)	3/4	0.411(1)	13.3(4)
O3	0.2348(5)	0.982(1)	0.4807(8)	5.4(2)
β-RbMgPO$_4$ (180 °C)				
Rb	−0.0026(4)	0.3080(1)	1/4	3.77(3)
Mg	0.3247(5)	0.5792(5)	0.260(1)	3.2(2)
P	0.2967(3)	0.4075(4)	0.7504(8)	3.4(1)
O1	0.200(2)	0.2781(8)	0.820(3)	9.7(7)
O2	0.4647(6)	0.401(1)	0.687(3)	13.4(6)
O3	0.248(1)	0.522(1)	0.939(2)	5.2(6)
O4	0.226(1)	0.458(1)	0.506(1)	2.5(4)
α-RbMgPO$_4$ (25 °C)				
Rb1	−0.0001(1)	0.2982(2)	1/4	1.50(5)
Rb2	0.1653(1)	0.1903(3)	0.2420(7)	1.86(7)
Rb3	0.1730(1)	0.8086(4)	0.7115(6)	1.95(8)
Mg1	0.1017(2)	0.5880(6)	0.232(1)	0.98(8)
Mg2	0.2819(3)	−0.0962(2)	0.242(1)	id.
Mg3	0.0517(3)	0.0608(7)	0.766(2)	id.
P1	0.0916(2)	0.3988(5)	0.737(1)	0.82(5)
P2	0.2726(2)	0.0892(5)	0.729(1)	id.
P3	0.0689(2)	0.9250(5)	0.216(1)	id.
O11	0.0613(4)	0.2636(9)	0.802(2)	0.76(6)
O12	0.1475(2)	0.374(1)	0.798(2)	id.
O13	0.0729(5)	0.514(1)	0.929(2)	id.
O14	0.0796(5)	0.441(1)	0.467(1)	id.
O21	0.2459(5)	0.2198(9)	0.851(2)	id.
O22	0.3276(2)	0.126(1)	0.760(3)	id.
O23	0.2629(5)	−0.037(1)	0.915(2)	id.
O24	0.2555(5)	0.052(1)	0.466(1)	id.
O31	0.0671(4)	0.7663(7)	0.298(2)	id.
O32	0.0171(3)	0.973(1)	0.113(2)	id.
O33	0.0868(5)	1.013(2)	0.449(2)	id.
O34	0.1039(4)	0.964(1)	0.995(2)	id.

Table 3
Selected bond lengths in the three forms of $RbMgPO_4$.

Bonds	d (Å)	Bonds	d (Å)
γ-RbMgPO$_4$ (220 °C)			
Rb–O3 (× 2)	3.017(6)	P–O3 (× 2)	1.526(6)
Rb–O3 (× 2)	3.124(7)	P–O1	1.54(1)
Rb–O1 (× 2)	3.273(8)	Mg–O2	1.761(7)
Rb–O2 (× 2)	3.397(7)	Mg–O1	1.85(1)
P–O2	1.523(5)	Mg–O3 (× 2)	1.898(7)
β-RbMgPO$_4$ (180 °C)			
Rb–O4	2.81(1)	Mg–O2	1.903(8)
Rb–O3	2.87(1)	Mg–O1	1.904(9)
Rb–O1	2.94(1)	Mg–O3	1.93(1)
Rb–O2	3.08(1)	Mg–O4	1.95(1)
Rb–O4	3.23(1)	P–O2	1.518(7)
Rb–O3	3.42(1)	P–O1	1.53(1)
Rb–O1	3.56(2)	P–O3	1.534(9)
Rb–O1	3.59(1)	P–O4	1.54(1)
α-RbMgPO$_4$ (25 °C)			
Rb1–O14	2.75(1)	P1–O14	1.53(1)
Rb1–O13	2.77(1)	P1–O11	1.53(1)
Rb1–O11	2.91(1)	P1–O12	1.537(7)
Rb1–O31	3.06(1)	P1-O13	1.56(1)
Rb1–O32	3.14(1)	P2–O22	1.51(1)
Rb1–O32	3.21(1)	P2–O24	1.52(1)
Rb1–O13	3.27(1)	P2–O21	1.55(1)
Rb1–O11	3.38(1)	P2–O23	1.56(1)
Rb1–O31	3.47(1)	P3–O31	1.54(1)
Rb1–O14	3.55(1)	P3–O34	1.55(1)
Rb2–O33	2.88(1)	P3–O32	1.55(1)
Rb2–O12	2.96(1)	P3–O33	1.56(1)
Rb2–O24	2.97(1)	Mg1–O22	1.915(8)
Rb2–O34	2.97(1)	Mg1–O13	1.92(1)
Rb2–O21	3.00(1)	Mg1–O31	1.93(1)
Rb2–O23	3.30(1)	Mg1–O14	1.95(1)
Rb2–O12	3.46(2)	Mg2–O23	1.90(1)
Rb2–O14	3.47(1)	Mg2–O12	1.917(8)
Rb3–O34	2.78(1)	Mg2–O21	1.95(1)
Rb3–O22	2.95(1)	Mg2–O24	1.95(1)
Rb3–O23	2.97(1)	Mg3–O11	1.91(1)
Rb3–O21	3.00(1)	Mg3–O33	1.98(1)
Rb3–O33	3.28(1)	Mg3–O32	2.02(1)
Rb3–O24	3.34(1)	Mg3–O34	2.05(1)
Rb3–O22	3.38(2)	Mg3–O32	2.22(1)
Rb3–O24	3.41(1)		
Rb3–O31	3.59(1)		

The cut-off distance for Rb–O bonds was set arbitrarily at 3.60 Å because of the very irregular shapes of the RbO_n polyhedra and the absence of clear gaps.

which is particularly strong for the O2 atom in the β- and γ-forms, is also probably responsible for the very low thermal expansion following the *a*-axis, nearly parallel to the P–O2–Mg linkages.

3.2. *β-RbMgPO$_4$*

This intermediate form occurs only in a narrow temperature domain. The Rietveld analysis of the 180 °C pattern was initiated with the same data set as for the γ form, but on the contrary, the absence of the *m*-mirror appeared clear enough to account for the polar space group $Pna2_1$ (Fig. 3, bottom).

3.3. *α-RbMgPO$_4$*

Surprisingly, the diffraction pattern of the low-temperature form does not exhibit the usual monoclinic modification. Although shifted compared to the β-form, the diffraction peaks are not splitted, accounting for the retention of the orthorhombic symmetry. Refining the structure on the basis of the β set was however unsatisfactory (R_{Bragg}=10.4); furthermore, numerous small peaks, non-existent in the β- and γ-forms remained unindexed. Several superstructure schemes were tested, until the cell was found, derived from the previous one by tripling the *a* parameter. Except for faint impurity peaks already existing in the patterns of the β- and γ-forms, the refinement in Le Bail's (profile matching) mode was successful. The systematic extinctions with the new indexing appeared to be still compatible with the previous space groups, so a test of second harmonic generation was made: under irradiation of a YAG:Nd laser (1.06 μm), the powder emitted a green light (0.53 μm), with a yield that could be estimated at about 50% of that of a KDP standard. This allowed us to conclude that $RbMgPO_4$ remains $Pna2_1$ at low temperature. The starting model was built by a three-fold expansion of the asymmetric unit of the β-form and refined (Fig. 4) with constraints on the P–O distances and common thermal factors for all the atoms of the same species, except for the rubidium. Finally, two of the Mg atoms still exhibited a tetrahedral coordination, whereas the third one appeared to be surrounded by five oxygen atoms forming an irregular square-base pyramid (Fig. 5). This partial change of coordination, allowed by a strong tilt of the PO_4 tetrahedron, can be held as responsible for the 3*a* superstructure. A similar change of coordination has been previously observed in parent phosphate $KMgPO_4$, but it only affects half of the Mg atoms, resulting in a two-fold superstructure at room temperature [12]. However, in the latter case, the structure becomes monoclinic.

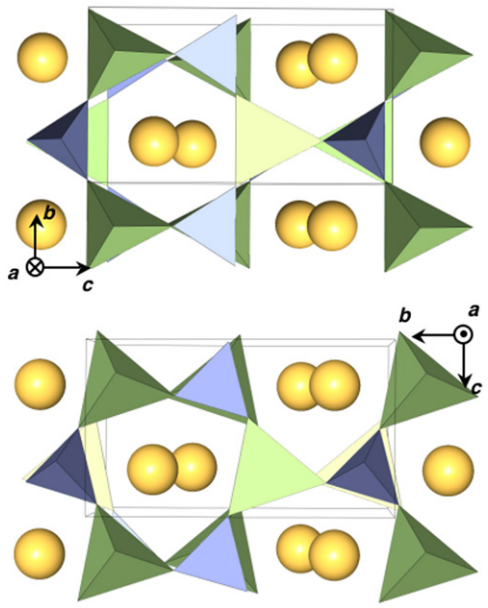

Fig. 3. (1 0 0) projections of γ-$RbMgPO_4$ (top) and β-$RbMgPO_4$ (bottom). Yellow: Rb atoms; green: MgO_4; blue: PO_4. Note the *m*-mirrors at $y=1/4$ and 3/4 in γ-$RbMgPO_4$. (For interpretation of the references to color in this figure legend, the reader is referred to the web version of this article.)

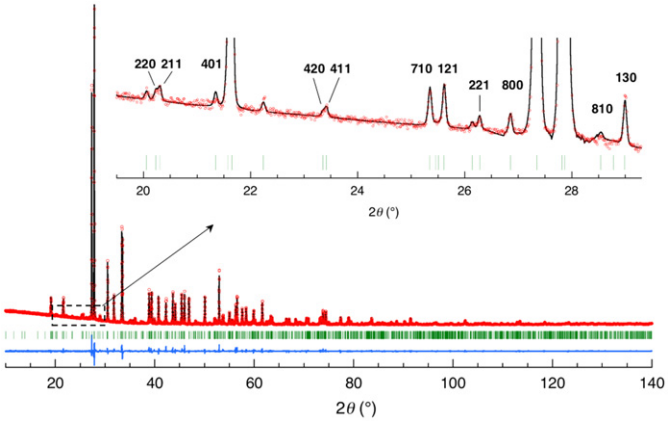

Fig. 4. Final Rietveld plot for α-$RbMgPO_4$. Red: observed intensities; black: calculated; blue: difference; bars: Bragg positions. The insert zooms on the superstructure peaks ($h \neq 3n$) generated by the tripling of the *a*-parameter. (For interpretation of the references to color in this figure legend, the reader is referred to the web version of this article.)

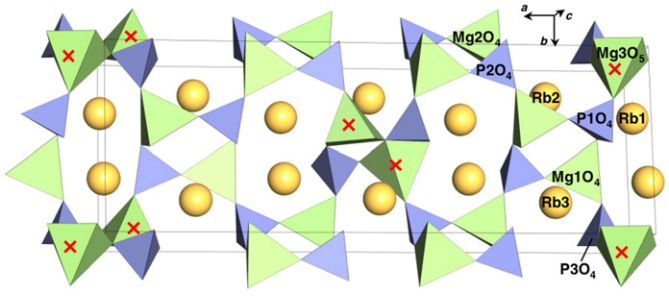

Fig. 5. Tilted (0 0 1) projection of α-$RbMgPO_4$. Note the tripling of the *a*-parameter resulting from the formation of $Mg3O_5$ pyramids (red marks). (For interpretation of the references to color in this figure legend, the reader is referred to the web version of this article.)

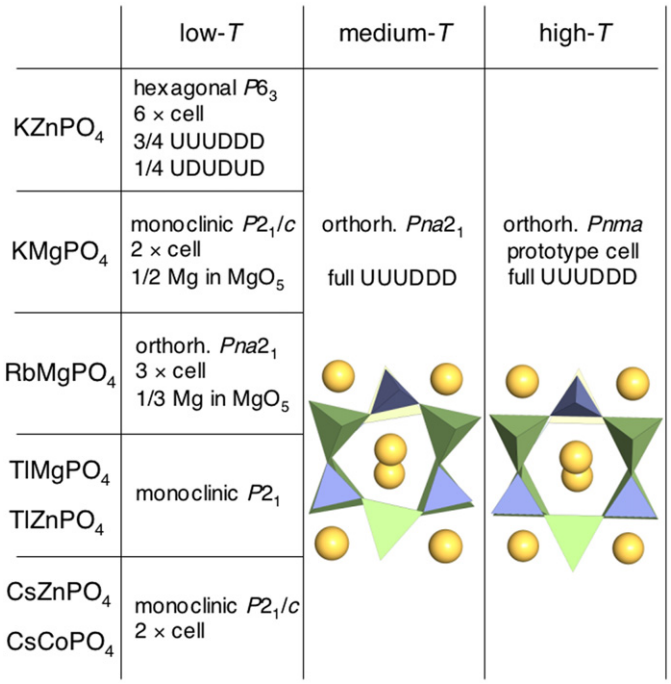

Fig. 6. The various low-temperature forms of stuffed tridymite monophosphates adopt the same medium- and high-temperature structures. The polymorphism of the Tl^{I} compounds is not fully demonstrated.

3.4. Polymorphism

Considering the faint thermal phenomenon at 169 °C, along with the small variations of the cell parameters and volume (0.3 $Å^3$, i.e., less than 0.07%), the β–γ transition appears as a typical second-order displacive phenomenon. The variation of the dielectric permittivity is also low. On the contrary, the change of coordination allows qualifying the α–β transition as a first-order one, with a moderate reconstructive character. Yet, the DTA signal is about 10 times more intense than that of the β–γ modification; likewise, the variation of the cell volume is strong (2.2 $Å^3$, 0.5%).

Among the numerous phosphates that adopt the stuffed tridymite type, few have sustained a complete analysis of their thermal behavior, but some conclusions can already be formulated. The existence of a *Pnma* high-temperature archetype with a subgroup $Pna2_1$ modification conform to Aizu's theory of phase transitions [14] appears as a common feature in this family. However, strong differences arise in the α-forms, indeed nearly as diverse as the compounds investigated till date (Fig. 6). At low temperature, steric and electronegativity factors prevail over symmetry concerns, thus resulting in divergent behaviors. Therefore, $KZnPO_4$ [15], like kalsilite $KAlSiO_4$ [16] tends to build UDUDUD rings that provide smaller coordination polyhedra for K^{I}. Even associated to a bigger cation like Cs^{I}, Zn^{II} remains in its usual tetrahedral environment and generates a low-temperature form very similar to the MT and HT ones. On the contrary, Mg^{II} rather obeys to steric criteria and increases its coordination, like in $KMgPO_4$ and $RbMgPO_4$. At last, the $Tl^{I}M^{II}PO_4$ phosphates, despite widely unknown, seem to exhibit an atypical behavior that could result from both the high covalency of the Tl–O bonds and the stereochemical effect of its $6s^2$ lone pair.

4. Conclusion

Previously unknown $RbMgPO_4$, although belonging to the stuffed tridymite family, presents an original low-temperature modification

that results from the tendency of tetrahedral Mg^{II} to increase its coordination. This polymorphism confirms the remarkably rich crystal chemistry of this still widely unknown family of monophosphates. As expected, the ferroelectric transition occurs at a moderate but positive temperature, but the dielectric effect is faint.

Acknowledgments

These research works have been developed under a bilateral research program Volubilis between the LCSM University Cadi Ayyad, Marrakech—Morocco and the LCPMC-UPMC Paris, France.

Appendix A. Supplementary materials

Supplementary data associated with this article can be found in the online version at doi:10.1016/j.jssc.2010.07.016.

References

[1] M. Andratschke, K.J. Range, H. Haase, U. Klement, Z. Naturforsch. B47 (1992) 1249.
[2] R. Masse, A. Durif, J. Solid State Chem. 73 (1988) 468.
[3] D. Blum, J.C. Peuzin, J.Y. Henry, Ferroelectrics 61 (1984) 265.
[4] D. Blum, A. Durif, M.T. Averbuch-Pouchot, Ferroelectrics 69 (1986) 283.
[5] N.Yu. Strutynska, I.V. Zatovsky, V.N. Baumer, N.S. Slobodyanik, Acta Crystallogr. E65 (2009) 58.
[6] G. Wallez, A. Elfakir, A.M. Xuriguera, M. Quarton, Powder Diffr. 8 (1993) 145.
[7] G. Wallez, S. Jaulmes, A. Elfakir, M. Quarton, J. Solid State Chem. 114 (1995) 123.
[8] A.I. Kruglik, M.A. Simonov, K.S. Aleksandrov, Kristallografiya 23 (1978) 494.
[9] W.A. Dollase, Acta Crystallogr. B25 (1969) 2298.
[10] K. Itoh, H. Ishikura, E. Nakamura, Acta Crystallogr. B37 (1981) 664.
[11] G. Wallez, S. Jaulmes, A. Elfakir, M. Quarton, J. Phys. III Fr. 4 (1994) 1197.
[12] G. Wallez, C. Colbeau-Justin, T. Le Mercier, M. Quarton, F. Robert, J. Solid State Chem. 136 (1998) 175.
[13] J. Rodriguez-Carvajal, FULLPROF.2k: Rietveld, profile matching and integrated intensity refinement of X-ray and neutron data, V 1.9c, Laboratoire Léon Brillouin, CEA, Saclay, France, 2001.
[14] K. Aizu, Phys. Rev. B2 (1970) 754.
[15] G. Wallez, F. Lucas, J.-P. Souron, M. Quarton, Mater. Res. Bull. 34 (1999) 1251.
[16] A.J. Perrotta, S.M. Smith, J.V. Smith, Miner. Mag. 35 (1965) 588.